Journal of Micromechanics and Microengineering

PAPER

Lithographically patterned polypyrrole multilayer microstructures via sidewall-controlled electropolymerization

To cite this article: Michael Synodis *et al* 2021 *J. Micromech. Microeng.* **31** 025008

IOP Publishing Journal of Micromechanics and Microengineering
J. Micromech. Microeng. **31** (2021) 025008 (10pp) https://doi.org/10.1088/1361-6439/abd098

Lithographically patterned polypyrrole multilayer microstructures via sidewall-controlled electropolymerization

Michael Synodis[1], Jun Beom Pyo[2], Minsoo Kim[2], Xuan Wang[2] and Mark G Allen[2]

[1] Department of Chemical and Biomolecular Engineering, University of Pennsylvania, Philadelphia, PA, United States of America
[2] Department of Electrical and Systems Engineering, University of Pennsylvania, Philadelphia, PA, United States of America

E-mail: mike.synodis@gmail.com

Received 3 October 2020, revised 20 November 2020
Accepted for publication 4 December 2020
Published 6 January 2021

Abstract

Composite materials comprising multilayers of metal and conductive polymer can have applications in sensing, biomedical, and energy storage/conversion scenarios. One attribute of such metal/polymer composites is that they typically display highly anisotropic electrical properties, which makes them useful as materials for microelectronic or magnetic devices. However, incorporating the deposition of conductive polymers into scalable and manufacturable fabrication processes can be challenging, as the mechanisms for electropolymerization are complex. We previously demonstrated an additive approach to fabricate metal/polymer multilayer structures, using soft magnetic alloys as the metal component and polypyrrole (PPy) as the polymer component. To extend the utility of these composites, the deposition of many multiples of alternating metal/polymer pairs within specifically defined lithographic molds is highly desirable. However, since the lateral growth of electrodeposited PPy is typically faster than vertical growth, non-uniform layer geometry and growth of the polymer on and above the patterned molds are often observed. In this work, we achieve suppression of lateral PPy growth by control of electropolymerization bath counter-anions and passivation of underlying metal layers during deposition. The lateral-to-vertical growth rate uniformity ratio is reduced by a factor of six (to approximately unity) through polymerization parameter optimization and exploiting a continuous five-bath electrodeposition approach. The reduction in lateral growth rate enhances the scalability of multilayer structures that are fabricated using this additive electrodeposition-based approach and provides a manufacturable route to additive, lithographically patterned metal/polymer composites with tunable volume and geometry, without sacrificing the microstructure and properties of the composite.

Keywords: electropolymerization, microstructures, composites, conductive polymers, microelectromechanical systems

(Some figures may appear in color only in the online journal)

1. Introduction

Conductive polymers, as a class of materials, can display a wide range of mechanical, electrical, and thermal properties, making them highly suitable for incorporation into microelectromechanical systems (MEMS). Such polymers can act as structural or active layers in supercapacitors or batteries [1–4], sensors [5–7], actuators [8–10], biocompatible devices

[11–13], and magnetic components [14–16]. As their electrical conductivities are typically intermediate between insulators and metals, conductive polymers have been investigated as interlamination materials in multilayer composites, the overall structure of which comprises alternating layers of metal and polymer [17]. Such composites have been shown to display anisotropic conductivities, where current flow through the structure is drastically different in the vertical and lateral directions. Such directed electrical properties are especially useful in magnetics and could be an enabler of on-chip miniaturized magnetic devices [18].

Sequential physical vapor deposition of metal and polymeric material can create structures with controlled individual layer thicknesses down to the nanoscale [19]; however, these approaches are often challenging to scale to larger total composite thicknesses due in part to relatively high built-in stress and long processing deposition times. As an alternative, electrodeposition-based multilayer processes provide the ability to control individual layer thicknesses as well as scalability to relatively large material volumes. While direct electrodeposition of metallic and insulating interlayer materials (which would be analogous to sequential physical vapor deposition) is not feasible due to the difficulty of electrodepositing a metal (or metal alloy) directly on a non-conducting material, development of additive approaches based on direct, non-vacuum-based deposition of a semi-insulating interlamination material (such as a conductive polymer) would make fabrication and exploitation of these composites more viable.

A major challenge to incorporating conductive polymers into composite materials with micron-scale feature sizes is depositing the polymer into patterned molds. Electropolymerization (analogous to electroplating) mechanisms for conductive polymers are complex, and the polymerization reactions often result in growth rates that are higher in the lateral direction due to the microstructural morphology of the polymer. High polymeric lateral growth coats the surface of lithographic molds (often overdepositing on the edges of the patterns), resulting in structures with non-uniform geometries, layer overlap, and potential loss of desired material properties.

In previous work, proof of concept magnetic laminations were fabricated using an additive, electrodeposition-based approach whereby a conductive polymer (polypyrrole (PPy)) was utilized as an insulating material within magnetic layers comprised of a nickel–iron alloy ($Ni_{80}Fe_{20}$, or permalloy) [17]. The electrical performance of these PPy–NiFe laminations was excellent, as the ratio of electrical conductivity in the lateral-to-vertical direction was over 10^6. However, the scalability of these structures was limited, as the lateral growth of PPy during electropolymerization resulted in large anisotropy in lamination thicknesses at the edges of the patterned multilayers as compared to the center. Thus, optimization of the PPy electropolymerization process is necessary to achieve a manufacturable route that avoids the use of larger molds for layer deposition (which are harder to fabricate) and also eliminates wasted material.

In this study, the mechanism for PPy electropolymerization is analyzed to guide polymerization bath compositions, layer deposition order, and deposition conditions, resulting in a process that can be utilized as a scalable additive fabrication approach for micro-scale multilayer composite materials within micromolds. The resulting structures were physically characterized to quantitatively assess the suppression of sidewall growth as well as ensure that proper layer anisotropy is maintained.

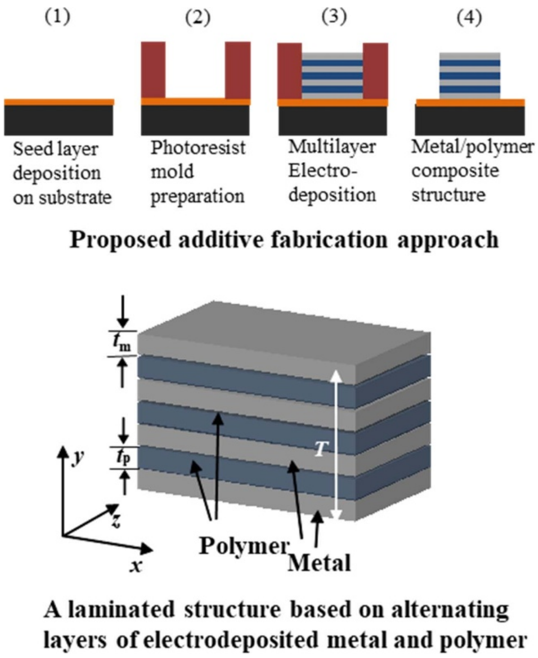

Figure 1. Top: schematics of a multilayer composite fabrication process based on sequential additive deposition. Bottom: a schematic of a laminated structure, including individual layer thicknesses of metal and polymer (t_m and t_p). The total thickness of the laminated structure is *T*.

2. PPy lamination fabrication

Figure 1 shows a schematic of an electrodeposition fabrication approach for the multilayer magnetic laminations discussed in [17]. The electropolymerization of the polymer insulating layer is completed in a deposition bath that consists of pyrrole monomer and a supporting electrolyte. The process occurs anodically and is initiated by the oxidation of a monomer molecule into a radical cation at the surface of the working electrode [20]. These monomer radicals can then react to form dimers that subsequently undergo dehydrogenation to form a stable species. During this process, anions in the supporting electrolyte migrate to the dimer site to maintain local charge neutrality and are thus incorporated with the chains as polymerization continues. During the initiation process, the supplied current must be sufficiently high that dimers and trimers can be formed at the surface of the working electrode before the radical monomers diffuse away or react with the electrolyte to form soluble products. Chains with two or more pyrrole monomer links are more stable after oxidation due to their ability to delocalize the radical across multiple rings. Termination of the polymerization reaction occurs when the current

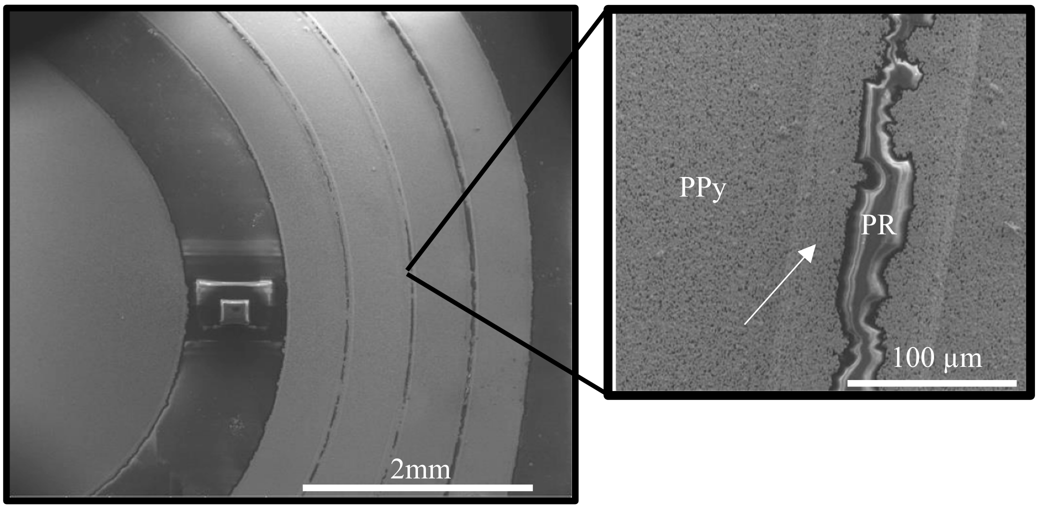

Figure 2. Top-down SEM images of PPy plated through a positive photoresist pattern of concentric toroids. Inset shows polymer overgrowth at the sidewalls of the pattern in the region indicated by the arrow, resulting from larger thicknesses at the edge as compared to the center. In this work, a supporting salicylate anion was utilized.

source is removed, and the further oxidation of monomer radicals ends [20].

During the fabrication of the structure illustrated in figure 1, it was found that the lateral electrical conductivity of the electropolymerized PPy was larger than its conductivity in the vertical direction [17]. Further, it was observed that as the monomer is polymerized, it grows outward to the edge of the conductive substrate and the insulating photoresist mold, at which point it grows laterally up the surface of the wall. It is hypothesized that the combination of enhanced conductivity and polymer morphology results in a larger driving force for growth in the lateral direction, thereby resulting in an increased thickness of electropolymerized polymer at the sidewalls. This non-uniformity can be quantitatively assessed by determining the ratio of the thickness of the deposited polymer layer at the edge of the pattern (t_{w}) to the thickness at the center (t_{c}). This measure of anisotropy is defined as α, as shown in equation (1):

$$\alpha = \frac{t_{\mathrm{w}}}{t_{\mathrm{c}}}. \tag{1}$$

A value of $\alpha = 1$ indicates uniform electrodeposition, while larger values of α suggest increasing non-uniformity. A typical α value measured for the standard PPy deposits discussed in previous work is approximately six, which leads to overplating.

Figure 2 shows typical results of electrodepositing PPy through a photoresist mold [17]. The deposition of polymer is demonstrated to be uniform across the area of the substrate, meaning that the polymer thickness was equal across the entire footprint; however, the uniformity in the vertical direction within each individual pattern was poor.

The large overgrowth at the edge of the patterns indicates the increased thickness of polymer at the photoresist wall interface due to lateral chain growth. In typical metal electrodeposition through a photoresist mold, the material growth is contained in the vertical direction and thickness uniformity ($\alpha = 1$) is observed. In general, high values of α indicate preferred growth of a material in the lateral direction during electrodeposition/polymerization (which leads to large peaks at the sides of patterns), while values approaching unity indicate preferred growth in the vertical direction (the typically desired state for electrodeposition through lithographically defined molds). In considering optimization of the polymer deposition process, the closeness of α to unity will be utilized as a key optimization parameter.

3. PPy electropolymerization optimization

3.1. Supporting anion optimization

In order to improve the electropolymerization performance of PPy interlamination layers, the mechanism of polymerization was considered. This analysis led to the formation of three main hypotheses: (a) the monomer concentration in the polymerization bath affects the extent of the anisotropy in the growth rates; (b) the type of anion used in the supporting electrolyte plays a role in the deposition type and ultimate properties of the resulting films [21, 22]; and (c) the current density used for deposition is crucial in controlling the reaction—there must be sufficient current supplied to initiate dimer formation and radicalization, but not so much that the difference in lateral growth rate due to large conductivity anisotropy of the deposited layers of PPy is enhanced. To test these hypotheses, a photoresist mold using the toroidal patterns shown in figure 2 is generated by spin casting AZ4620 positive resist (MicroChem) on a 2 × 3 inch glass substrate coated with a seed layer of sputtered Ti/Au (50 nm/100 nm). After developing the patterns (~4 cm^2 surface area toroidal patterns with varying widths) into the photoresist, pyrrole is electropolymerized through the mold using various bath compositions and current conditions, and the resulting film is characterized via profilometry for thickness (and α calculation) and optical and SEM microscopy for structural uniformity. Additionally, deposition

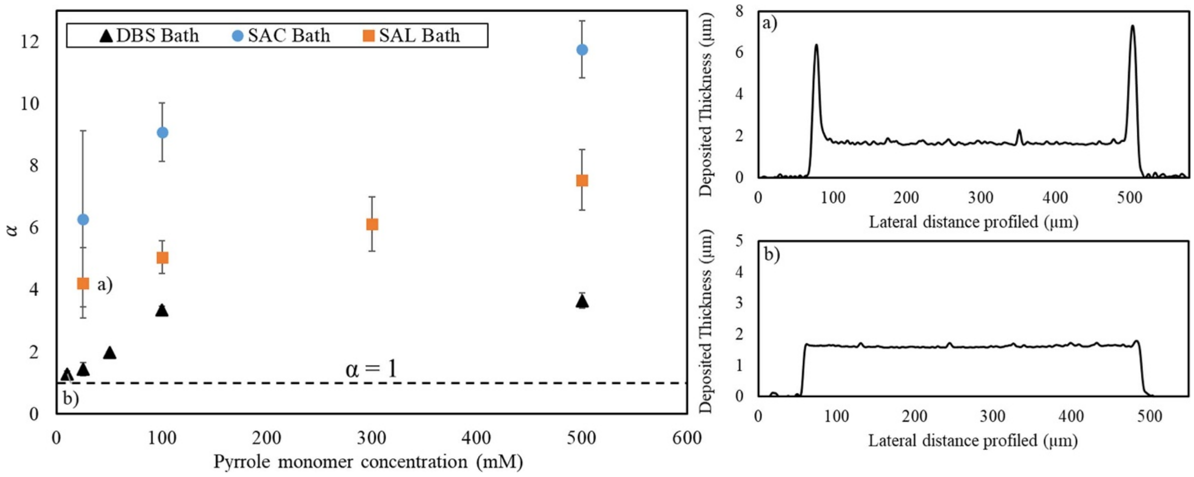

Figure 3. Pattern wall to pattern center thickness ratios (α) as a function of monomer concentration, parameterized by the type of anion in the polymerization bath. Anion concentration was kept constant at 100 mM. Insets (a) and (b) illustrate example thickness profiles of two 500 μm wide patterned films, using SAL (data point (a) on the left plot) and DBS baths (data point (b) on the left plot), respectively, with 25 mM monomer concentration. The horizontal line at $\alpha = 1$ on the left plot indicates the optimization goal.

voltage profiles and compatibility with NiFe plating and Ni surface activation are measured.

The anions used in this study, salicylate (as sodium salicylate or NaSAL), dodecylbenzensulfonate (as NaDBS), and saccharin (as NaSac), were obtained from Aldrich, Inc. and used as received. These supporting electrolyte salts are some of the most commonly used in PPy manufacturing [23–27]. Pyrrole monomer was obtained from Aldrich, Inc. and vacuum distilled prior to use. Polymerization baths were prepared by adding appropriate quantities of pyrrole to an aqueous solution of freshly dissolved supporting electrolyte. A parametric study of monomer concentrations as well as supporting anion type was conducted to identify both the anion and bath conditions that lead to optimal growth rates. The concentration of the pyrrole monomer was adjusted for each bath while maintaining the anion concentration constant, such that the effects of the type of anion as well as of the monomer amount could be analyzed.

To determine the value of α for each parametric condition, electrodeposition of a single layer of PPy proceeded through the test photoresist molds described above, following similar fabrication procedures as described in [17]. Briefly, mold thicknesses of 10–12 μm were utilized, and 1 μm electrodeposited PPy thicknesses were targeted, ensuring that the value of α could be measured for each condition regardless of the growth conditions achieved for a particular sample. After the electropolymerization was completed, the photoresist molds were removed, and profilometry of the resultant deposited films was performed to assess the level of anisotropic growth. Figure 3 shows raw data scans of high and low α value films, as well as the results of the parametric study, α values parameterized by anion type, and monomer concentration. A clear trend in the data is evident, indicating that reducing the ratio of the monomer concentration to the anion concentration results in reducing α for that particular bath combination. Additionally, the DBS anion clearly yields the lowest α values among the anions and conditions studied.

At the lowest monomer concentrations (10 mM and 25 mM), the DBS bath enables the reduction of α to approximately 1.2, which is close to the optimally flat condition of $\alpha = 1$. This is highlighted by the insets in figure 3, where image (a) shows large peaks in the film profile at the pattern edge due to lateral growth of PPySAL and a high α, whereas image (b) shows the flat profile with low α achieved using PPyDBS. A possible mechanism for the reduction of α using DBS (compared to the salicylate and saccharin anions) is that the long carbon chain provides steric hindrance to lateral growth of the monomer chains [28]. NaDBS, as a surfactant, forms energetically favorable micelle-like configurations around the monomer molecules as they are diffusing to the surface of the working electrode. Upon oxidative polymerization, these long chains provide a barrier to growth in the lateral direction and thus greatly reduce the anisotropy in thickness toward the edge of a patterned mold in comparison to the center. This effect, combined with a reduction in the overall monomer concentration in the polymerization bath, can suppress the lateral growth of the PPy films. The salicylate and saccharin ions, conversely, do not exhibit this steric hindrance, and thus demonstrate α values in the four to six range even at low monomer concentrations.

3.2. *Multilayer fabrication optimization*

In order to determine the efficacy of using the various anion-doped polymers in a multilayer construct, sample metal/polymer test structures were fabricated, using NiFe as the test metal, similar to the composites described in [17]. Briefly, a toroidal photoresist mold was prepared on a 2×3 inch glass substrate coated with a seed layer of sputtered Ti/Au (50 nm/100 nm). A 20 μm thick photoresist pattern was developed on the surface of the substrate, and a structure consisting of NiFe, PPy, an optional activation layer (Ni strike) to facilitate metal deposition on PPy, and NiFe, was deposited through the mold via sequential electrodeposition.

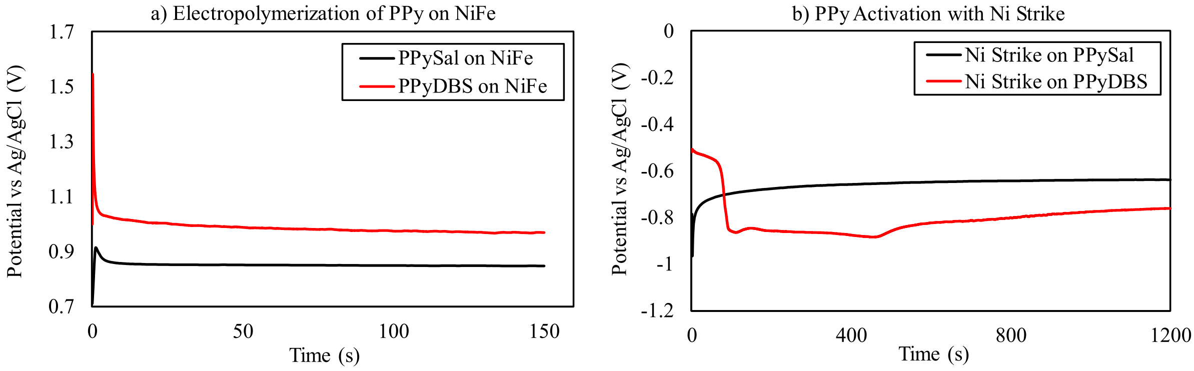

Figure 4. Voltage deposition profiles versus electrodeposition time for (a) PPy electropolymerization, and (b) Ni strike activation with both SAL and DBS electrolytes.

Target thicknesses for each layer were again 1 μm (except for the activation layer, which is$\sim$100 nm), such that the growth anisotropy could be measured. The electrodeposition voltage profiles were monitored during various steps in the overall fabrication process, as shown in figure 4.

The deposition characteristics with the DBS-based bath were first compared to deposition with the SAL bath (figure 6(a)). At a typical current density of 2.5 mA cm^{-2}, the deposition potentials of PPyDBS and PPySAL were stabilized at approximately $+1$ V and $+0.87$ V, respectively, relative to Ag/AgCl; however, a large activation peak can be seen with the DBS anion, which is hypothesized to be due to underlying corrosion of the NiFe substrate layer.

The salicylate head group is able to form a complex with active metals that prevents their complete oxidation during the initiation of the anodic polymerization process. This has been demonstrated in the literature by cyclic voltammetry experiments performed with salicylate anions on active metals such as zinc and copper [29]. It is hypothesized that this complexing effect reduces the initial voltage peak during polymerization and slightly passivates the underlying metal surface until complete coverage of the surface with polymer is achieved.

Surface activation of the PPy layer with a low potential Ni strike was also tested with PPy films deposited with both SAL and DBS anions (figure 5(b)). At the initial stage of deposition, the Ni reduction onto the PPyDBS surface occurs at a significantly lower potential compared to the deposition on the PPySAL, but the Ni deposition potential on the PPyDBS gradually increases beyond the PPySAL potential. The initial low Ni deposition potential of PPyDBS corresponds to the potential measured on a bare NiFe surface (-0.543 V, 0.1 s after the deposition began). Thus, it is hypothesized that the Ni deposition reaction could occur not only on the PPyDBS, but also from the surface of the previously deposited NiFe layer. As a result, it was observed that attempts to deposit Ni or NiFe on a DBS surface would result in dendritic or bead-like growth that would not be suitable for subsequent layer deposition (as shown in figure 5).

During deposition of Ni on the PPySAL surface, as the thickness of the Ni film increases, the resistance of the substrate decreases (due to Ni conductivity being much larger than that of PPy), and the deposition potential decreases as well. The smooth deposition profile indicates that there are no areas of local Ni deposition directly on the NiFe surface, and the lower deposition potential of PPySAL on NiFe in figure 5(a) indicates the passivation of the NiFe surface. The result of these two phenomena, as shown in the optical images contained in figures 5 and 6, is that successful multilayer laminations are enhanced by a Ni strike activation on the surface of a PPySAL polymeric layer.

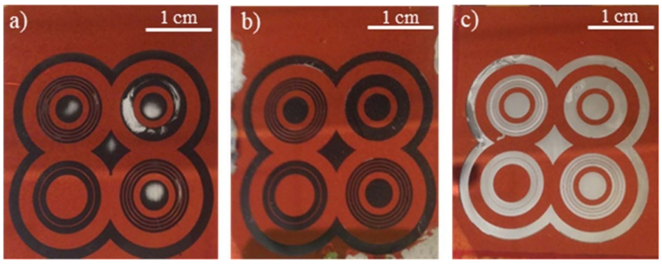

Figure 5. Top-down optical images of a sample toroidal patterned area after (a) NiFe on PPySAL, (b) NiFe on PPyDBS, and (c) NiFe on Ni on PPySAL.

The images in figure 6 demonstrate that permalloy deposition is not successful through direct deposition on PPyDBS or PPySAL, but rather only through depositing PPySAL, activated with Ni, and then depositing the NiFe (figure 5(c)). In figure 5, optical images show the uniformity of metal deposits on top of the polymer surfaces. Figure 6(a) shows an image of a Ni strike layer on a PPyDBS surface. As mentioned previously, only islands of Ni form through the polymer layer, as the porosity of the DBS films increases the ability of the Ni to deposit directly on the underlying NiFe layer. Figures 6(b) and (c) show uniform Ni and NiFe deposition on PPySAL, thus confirming that the complexing effect of the SAL anion as well as the denser resulting polymer films facilitate multilayer lamination fabrication. Note that in figure 6(c) it is also clear that there is more deposition at the edges of the pattern, confirming the high α characteristic of the PPySAL deposition.

Given the characteristics of all tested anions, combining the properties of the DBS and SAL baths, either directly or as multiple separate depositions within a single PPy layer, could lead to uniform multilayer deposition with low α value. To this end, a set of experiments was performed in which proof of concept

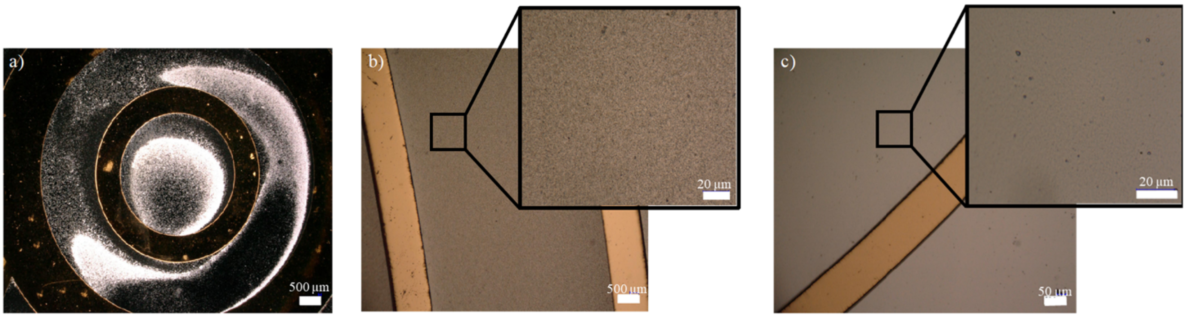

Figure 6. Top-down, optical images of multilayer structures after metal deposition. Image (a) is Ni strike on NiFe–PPyDBS multilayer, (b) is Ni strike on NiFe–PPySAL multilayer, and (c) is NiFe on Ni strike on PPySAL–NiFe multilayer. Note, the insets in (b) and (c) provide images of the films at higher magnification, demonstrating uniformity and lack of porosity on a micro-scale.

Table 1. Summary of mixed DBS and SAL deposition experiments.

Bath type	DBS conc (M)	SAL conc (M)	PPy conc (M)	Current density (mA cm^{-2})	α average	α st. dev.
DBS only	0.1	0	0.01	0.3	1.1	0.04
SAL, low *J*	0	0.1	0.3	0.3	2.7	0.9
SAL, med *J*	0	0.1	0.3	1	4.7	0.9
SAL, high *J*	0	0.1	0.3	2.5	5.2	2.2
SAL pulse low	0	0.1	0.3	2.5 (0.1 s on, 1 s off)	2.3	1.1
SAL pulse high	0	0.1	0.3	2.5 (0.1 s on, 10 s off)	1.8	0.5
Mixed DBS SAL	0.3	0.3	0.3	1	1.4	0.2
DBS + SAL strike	0.1	0.1	(0.01, 0.3)	0.3, 2.5	1.3	0.1
DBS, SAL, Ni, NiFe	0.1	0.3	(0.01, 0.3)	0.3, 2.5, 0.5, 10	1.4	0.3

NiFe/PPy/NiFe multilayer structures were fabricated (using the same procedure as described above) while varying the composition of the electropolymerization bath as well as the deposition conditions. Deposition solutions were tested with DBS anions alone, SAL anions alone, and a mixture of both, while also varying the anion concentrations and deposition current densities. In addition to an anionic mixture, sequential deposition of PPy films from individual baths with different anions were also tested. The data collected from each test consisted of an α measurement for a single PPy layer as well as a qualitative review of the compatibility of the specific parameters with scalable multilayer fabrication. Table 1 summarizes the experimental conditions investigated as well as the resultant values of α. Five tests were repeated for each bath type.

Several conclusions can be drawn from the data in table 1. First, changing the current density of a PPySAL deposition while keeping the monomer concentration high is insufficient to minimize the lateral growth rate. However, utilizing pulse deposition at the same monomer concentration and current density resulted in a reduced α value of 1.8. Additionally, using a combination layer of PPyDBS first with a thin PPySAL strike on top further decreased α to between 1.3 and 1.4. While using a bath with a mixture of DBS and SAL ions in the solution resulted in a similar α value, Ni strike activation on the resulting polymer surface failed, indicating that it is necessary to have a corrosion-free substrate as well as a pure PPySAL surface for the activation toward multilayer deposition in this system.

While the value of α did not appear to directly affect the properties of the resulting polymerized films, it has been shown that the choice of anion can impact their characteristics (e.g. the electrical conductivity) [30–32]. Investigation of such electrical or mechanical properties was outside the scope of this work.

3.3. Optimized fabrication results

Given the results shown in table 1, finding the optimal PPy polymerization solution and deposition conditions for multilayer electrodeposition through lithographically patterned molds required a balance of minimizing α for the polymer film, ensuring good uniformity and contact during the multilayer plating process, and consideration of fabrication time and complexity for each step. For example, both the plating rate and α decrease for the polymer layer with decreasing applied current density, yet a minimum threshold of current is necessary to apply a uniform layer of the polymer on the metal surface before it is damaged during the anodic polymer deposition conditions. The anion incorporated into the polymer film also impacts the plating rate, α value, and the compatibility with the subsequent metal deposition.

Table 2. Process summary for batch fabrication of multilayer polymer/metal composites.

Process step	Material deposited	Deposition bath	Deposition conditions
1	NiFe	Nickel sulfate, nickel chloride, boric acid, saccharin	Cathodic, 10 mA cm^{-2}
2	Au	Transene sulfite gold commercial solution	Cathodic, 2 mA cm^{-2}, 60 °C
3	PPyDBS	Pyrrole monomer, sodium dodecylbenzenesulfonate	Anodic, 0.25 mA cm^{-2}
4	PPySAL	Pyrrole monomer, sodium salicylate	Anodic, 2.5 mA cm^{-2} pulses
5	Ni	Nickel chloride anhydrous, boric acid, saccharin	Cathodic, 0.5 mA cm^{-2}, 46 °C–50 °C

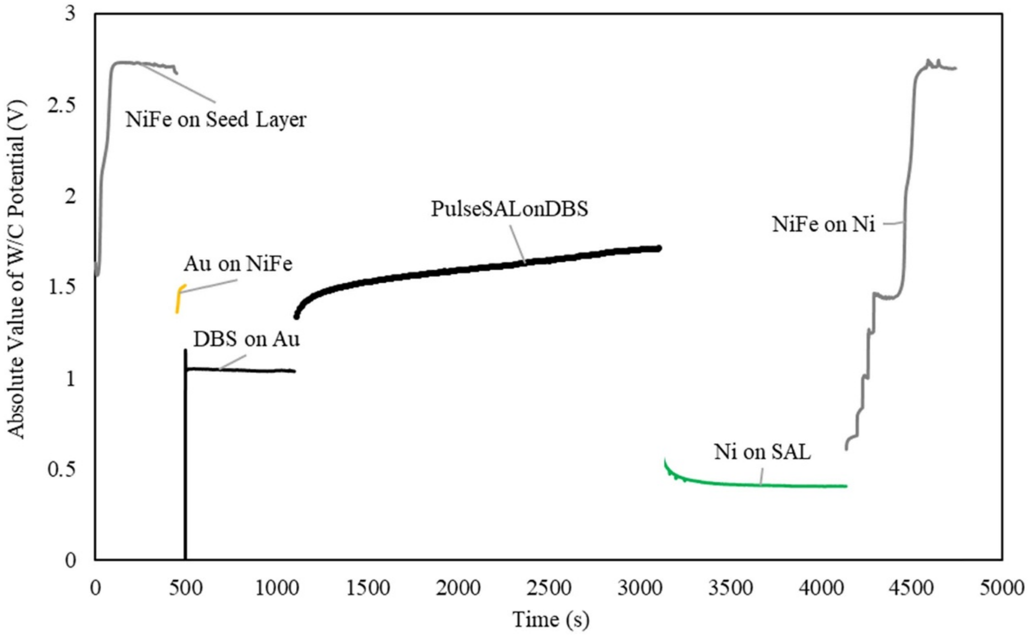

Figure 7. Deposition profiles for all layers in the optimized five-bath electrodeposition scheme. The potential was measured between the working and counter electrodes (W/C) for each electrodeposition/electropolymerization step.

Based on these observations and constraints, a multilayer deposition procedure comprising a five-step plating process was designed. This process not only achieved good interfaces between the metal and polymer layers, but also achieved good in-mold uniformity. The process steps for each set of layers to form a composite stack are listed in table 2. This set of processes could be repeated to form many multilayers within a single mold.

In the process described in table 2, the cathodic NiFe deposition controls the magnetic layer thickness, a thin gold layer is deposited on top of the NiFe to prevent corrosion during subsequent polymer deposition, a thick PPyDBS film is electropolymerized for insulation and good α characteristics, a thin PPySAL layer is pulse electropolymerized for introduction of the activation surface, and a Ni strike layer is cathodically plated for activation of the PPySAL surface for the next magnetic layer deposition. A current density of 0.3 mA cm^{-2} for the PPyDBS deposition provided a balance between achieving a low α value while still maintaining a reasonable fabrication time for that step in the process. The pulse PPySAL provides an activated surface for subsequent metal deposition without resulting in an increased overall α for the structure. A sample deposition voltage profile is shown in figure 7.

As seen in figure 7, the deposition profiles are very similar to the single layer experiments, except in the case of the pulse deposition of PPySAL, where a 1:100 duty cycle was used. It is important to note that the Ni activation on the pulse-deposited PPySAL layer occurs quickly and at low potential, and that after a ramp-up of current density the second NiFe magnetic layer deposition occurs at the same potential as the initial layer coated on top of the sputtered seed metal. This indicates that a robust process has been established, which is further validated by the optical and SEM images shown in figure 8.

Figure 8(a) shows the actual plated toroidal sample after multiple sets of the five-bath process have been completed. The uppermost layer in figure 8 is NiFe. Excellent plating uniformity across the patterned area of the mold is observed, with no obvious delamination after photoresist removal. Figure 8(b) shows an optical microscope image of the multi-anion PPy insulation layer after both DBS and SAL electropolymerization. The image shows a smooth surface as well as no visible growth at the edges of the pattern. Figure 8(c) shows the top NiFe surface on the same pattern after multiple five-bath sets have been completed. Again, the plated layers are smooth and show no indication of lateral growth impact. Lastly, in figure 8(d), a focused ion beam/SEM cross-sectional image is shown, highlighting the smooth and distinct PPy and NiFe

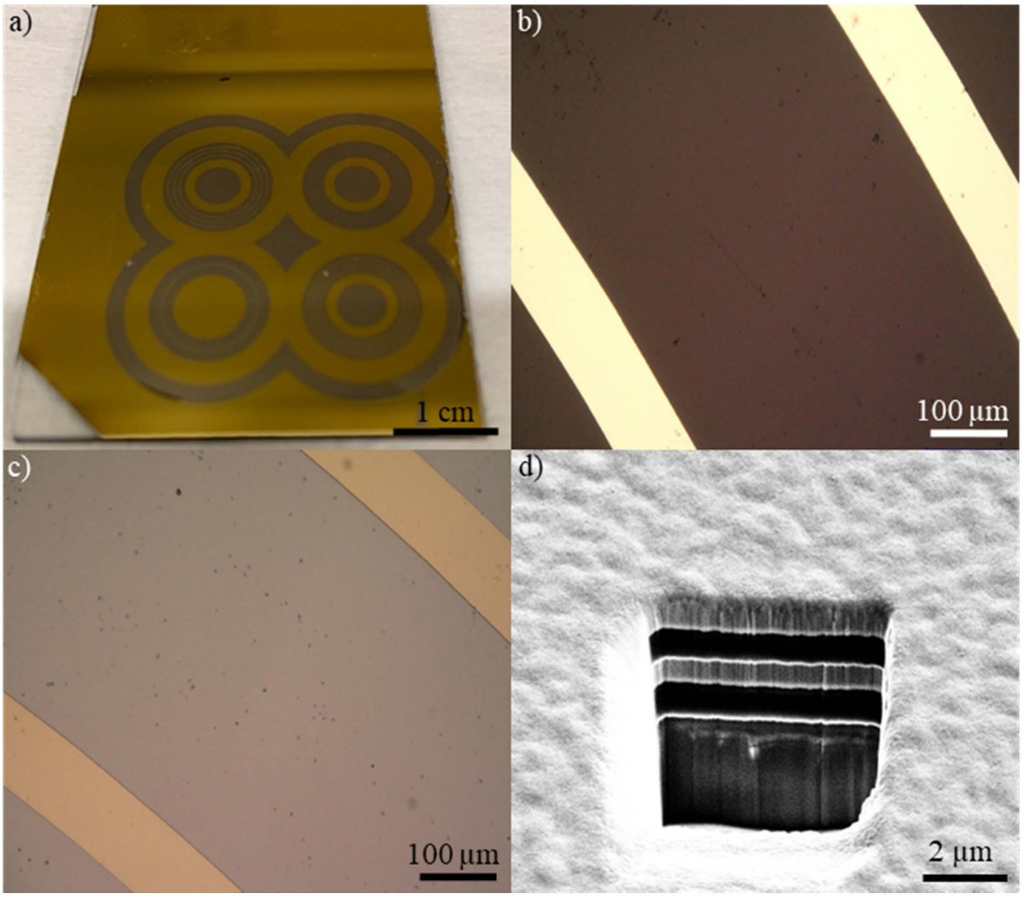

Figure 8. Optical and SEM images of laminated structures generated by the optimized five-bath deposition scheme. (a) Top-down view of test mask after multilayer plating, (b) optical microscope image of the multi-anion PPy insulating layer, (c) optical microscope image of the top layer of NiFe after two sets of the five baths were completed, and (d) a focused ion beam/SEM cross-sectional image highlighting the distinct multilayer laminated sets.

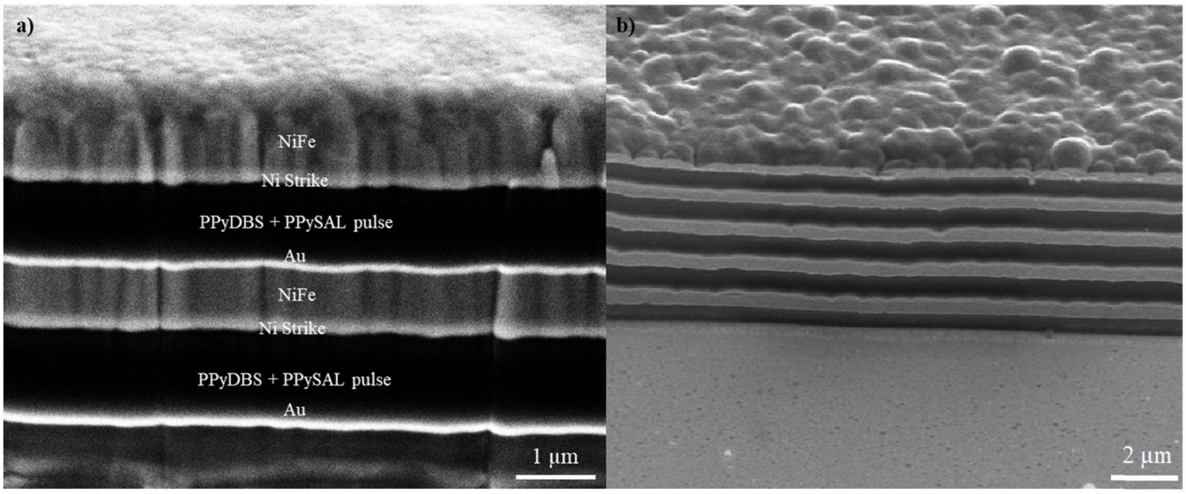

Figure 9. (a) A magnified focused ion beam/SEM cross-sectional image of a two-set laminated stack using the optimized five-bath multilayer electrodeposition process. The layer corresponding to each bath in the set is labeled. (b) An SEM cross-sectional image at the edge of a patterned lamination (where the photoresist wall once was), indicating minimized lateral growth of the polymer layers and increased multilayer uniformity.

laminations after multilayer electrodeposition. In figure 9(a), a magnified version of figure 8(d) is provided, where each of the five layers in the set is identified.

As seen in the magnified cross-section, the ∼100 nm thick gold protection layer prevents damage to the NiFe active layer during PPy electropolymerization, and a uniform Ni strike

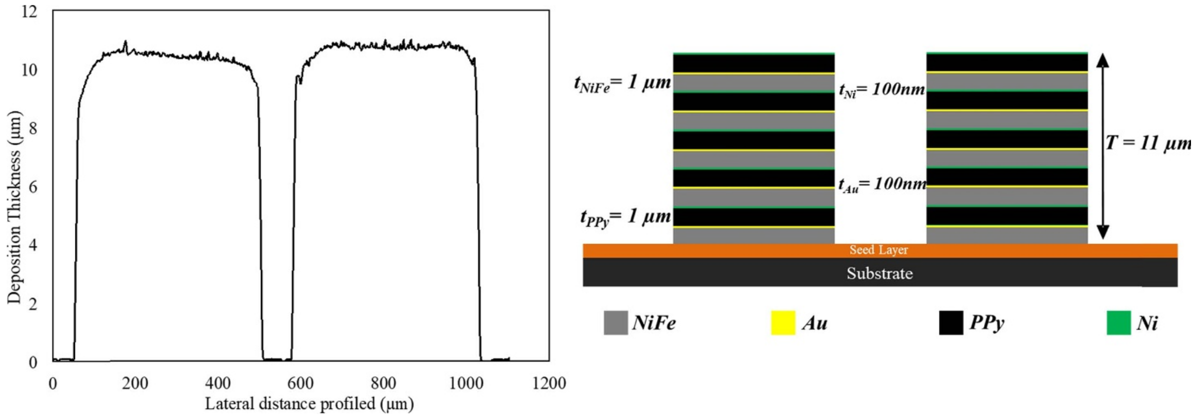

Figure 10. Sample profilometry data for a five-set patterned multilayer laminated structure, where each set consists of NiFe–Au–PPyDBS–PPySAL–Ni constructs. A schematic of the measured patterned multilayer structure is shown on the right. The metal and polymer layer thicknesses were optimized (via deposition conditions) to be 1 μm each, resulting in a total laminated structure approximately 11 μm thick Note that peaks that would indicate lateral polymer growth during deposition are absent in the profilometry data.

activation layer is achieved on the multi-anion PPy insulation set, resulting in multiple successful NiFe plated layers. After all layers in the set were deposited, sample thicknesses were measured in the profilometer to determine α.

It was found that for the individual PPy layer $\alpha_{\mathrm{ave}} = 1.2 \pm 0.08$, and for the overall sets $\alpha_{\mathrm{ave}} = 1.15 \pm 0.14$. This is evident in figure 9(b), which shows the absence of excess layer thickness in a cross-section at the sidewall, where the photoresist mold was removed. A sample profilometry scan of a five-set multilayer lamination is provided in figure 10, in which the lack of peaks at the edge of the pattern walls (as compared to figure 3(a)) demonstrates the suppression of polymer lateral growth during electropolymerization in all layer sets.

These results indicate that using a combination of PPyDBS and PPySAL layers was successful in enabling multilayer structure scaling while maintaining excellent α performance. The combination of these characteristics will enable the manufacture of multilayer metal/polymer composites with scalable volume while maintaining beneficial structural properties due to micro-scale layer thicknesses and material anisotropies.

4. Conclusions

A five-bath sequential multilayer deposition fabrication technique was developed to optimize the fabrication of PPy/permalloy composite materials. In particular, the use of sidewall-controlled electropolymerization of PPy via multi-step and multi-anion deposition solutions enables structures with scalable overall volumes and simultaneously tunable (and lithographically patterned) geometries. This additive, aqueous-based fabrication technology could advance the commercialization capabilities of electrodeposited conductive polymer composites, and further provides a manufacturable route to materials with anisotropic mechanical and/or electrical properties that provide utility in MEMS sensing, energy, and/or biomedical applications.

Acknowledgments

This work was carried out in part at the Singh Center for Nanotechnology, which is supported by the NSF National Nanotechnology Coordinated Infrastructure Program under Grant No. NNCI-2025608. The authors also acknowledge the financial support of EnaChip, Inc., and declare a financial interest therein.

ORCID iDs

Michael Synodis https://orcid.org/0000-0002-2157-2265
Minsoo Kim https://orcid.org/0000-0001-5280-2994

References

[1] Fan L Z and Maier J 2006 High-performance polypyrrole electrode materials for redox supercapacitors *Electrochem. Commun.* **8** 937–40

[2] Huang Y, Li H, Wang Z, Zhu M, Pei Z, Xue Q, Huang Y and Zhi C 2016 Nanostructured polypyrrole as a flexible electrode material of supercapacitor *Nano Energy* **22** 422–38

[3] Eftekhari A, Li L and Yang Y 2017 Polyaniline supercapacitors *J. Power Sources* **347** 86–107

[4] Min H S, Park B Y, Taherabadi L, Wang C, Yeh Y, Zaouk R and Dunn B 2008 Fabrication and properties of a carbon/polypyrrole three-dimensional microbattery *J. Power Sources* **178** 795–800

[5] Collins G E and Buckley L J 1996 Conductive polymer-coated fabrics for chemical sensing *Synth. Met.* **78** 93–101

[6] Liu H *et al* 2018 Electrically conductive polymer composites for smart flexible strain sensors: a critical review *J. Mater. Chem.* C **6** 12121–41

[7] Herrmann S, Ritchie C and Streb C 2015 Polyoxometalate—conductive polymer composites for energy conversion, energy storage and nanostructured sensors *Dalton Trans.* **44** 7092–104

[8] Okuzaki H, Takagi S, Hishiki F and Tanigawa R 2014 Ionic liquid/polyurethane/PEDOT:PSS composites for electro-active polymer actuators *Sensors Actuators* B **194** 59–63

[9] Shklovsky J, Reuveny A, Sverdlov Y, Krylov S and Shacham-Diamand Y 2018 Towards fully polymeric electroactive micro actuators with conductive polymer electrodes *Microelectron. Eng.* **199** 58–62

[10] Ren K, Liu S, Lin M, Wang Y and Zhang Q M 2008 A compact electroactive polymer actuator suitable for refreshable Braille display *Sensors Actuators* A **143** 335–42

[11] Kim D H, Wiler J A, Anderson D J, Kipke D R and Martin D C 2010 Conducting polymers on hydrogel-coated neural electrode provide sensitive neural recordings in auditory cortex *Acta Biomater.* **6** 57–62

[12] Nambiar S and Yeow J T 2011 Conductive polymer-based sensors for biomedical applications *Biosens. Bioelectron.* **26** 1825–32

[13] George P M, Lyckman A W, LaVan D A, Hegde A, Leung Y, Avasare R and Sur M 2005 Fabrication and biocompatibility of polypyrrole implants suitable for neural prosthetics *Biomaterials* **26** 3511–9

[14] Resta I M, Horwitz G, Elizalde M L M, Jorge G A, Molina F V and Antonel P S 2013 Magnetic and conducting properties of composites of conducting polymers and ferrite nanoparticles *IEEE Trans. Magn.* **49** 4598–601

[15] Gu H *et al* 2014 Magnetoresistive conductive polymer–tungsten trioxide nanocomposites with ultrahigh sensitivity at low magnetic field *Polymer* **55** 944–50

[16] Shalygina E E, Kharlamova A M, Makarov A V, Vorobieva N V and Lachinov A N 2018 Peculiarities of the magnetic properties of thin-film three-layer Fe/Poly (diphenylene phthalide)/Fe systems *J. Magn. Magn. Mater.* **459** 328–30

[17] Synodis M, Pyo J B, Kim M, Oh H, Wang X and Allen M G 2020 Fully additive fabrication of electrically anisotropic multilayer materials based on sequential electrodeposition *J. Microelectromech. Syst.* **29** 1510–7

[18] Kim J, Kim M, Herrault F, Park J Y and Allen M G 2014 Electrodeposited nanolaminated CoNiFe cores for ultracompact DC–DC power conversion *IEEE Trans. Power Electron.* **30** 5078–87

[19] Yao D, Levey C G, Tian R and Sullivan C R 2013 Microfabricated V-groove power inductors using multilayer Co–Zr–O thin films for very-high-frequency DC–DC converters *IEEE Trans. Power Electron.* **28** 4384–94

[20] Sadki S, Schottland P, Brodie N and Sabouraud G 2000 The mechanisms of pyrrole electropolymerization *Chem. Soc. Rev.* **29** 283–93

[21] Ansari R 2006 Polypyrrole conducting electroactive polymers: synthesis and stability studies *J. Chem.* **3** 186–201

[22] Ruangchuay L, Sirivat A and Schwank J 2004 Electrical conductivity response of polypyrrole to acetone vapor: effect of dopant anions and interaction mechanisms *Synth. Met.* **140** 15–21

[23] Qi K, Qiu Y, Chen Z and Guo X 2012 Corrosion of conductive polypyrrole: effects of environmental factors, electrochemical stimulation, and doping anions *Corros. Sci.* **60** 50–58

[24] Bazzaoui M, Martins J I, Costa S C, Bazzaoui E A, Reis T C and Martins L 2006 Sweet aqueous solution for electrochemical synthesis of polypyrrole: part 1-A. On non-ferrous metals *Electrochim. Acta* **51** 2417–26

[25] Fenelon A M and Breslin C B 2002 The electrochemical synthesis of polypyrrole at a copper electrode: corrosion protection properties *Electrochim. Acta* **47** 4467–76

[26] Prissanaroon W, Brack N, Pigram P J and Liesegang J 2004 Electropolymerisation of pyrrole on copper in aqueous media *Synth. Met.* **142** 25–34

[27] Bazzaoui M, Martins J I, Bazzaoui E A, Reis T C and Martins L 2004 Pyrrole electropolymerization on copper and brass in a single-step process from aqueous solution *J. Appl. Electrochem.* **34** 815–22

[28] Naoi K, Oura Y, Maeda M and Nakamura S 1995 Electrochemistry of surfactant-doped polypyrrole film (I): formation of columnar structure by electropolymerization *J. Electrochem. Soc.* **142** 417–22

[29] Petitjean J, Aeiyach S, Lacroix J C and Lacaze P C 1999 Ultra-fast electropolymerization of pyrrole in aqueous media on oxidizable metals in a one-step process *J. Electroanal. Chem.* **478** 92–100

[30] Kupila E L and Kankare J 1993 Electropolymerization of pyrrole: effects of pH and anions on the conductivity and growth kinetics of polypyrrole *Synth. Met.* **55** 1402–5

[31] Otero T F and Martinez J G 2014 Structural electrochemistry: conductivities and ionic content from rising reduced polypyrrole films *Adv. Funct. Mater.* **24** 1259–64

[32] Benslimane M, Gravesen P, West K, Bay L and Skaarup S 2000 Conducting polymer materials and their mechanical properties *Proc. the 7th Int. Conf. New Actuators January 1, 2000 Bremen, Germany* pp 635–8